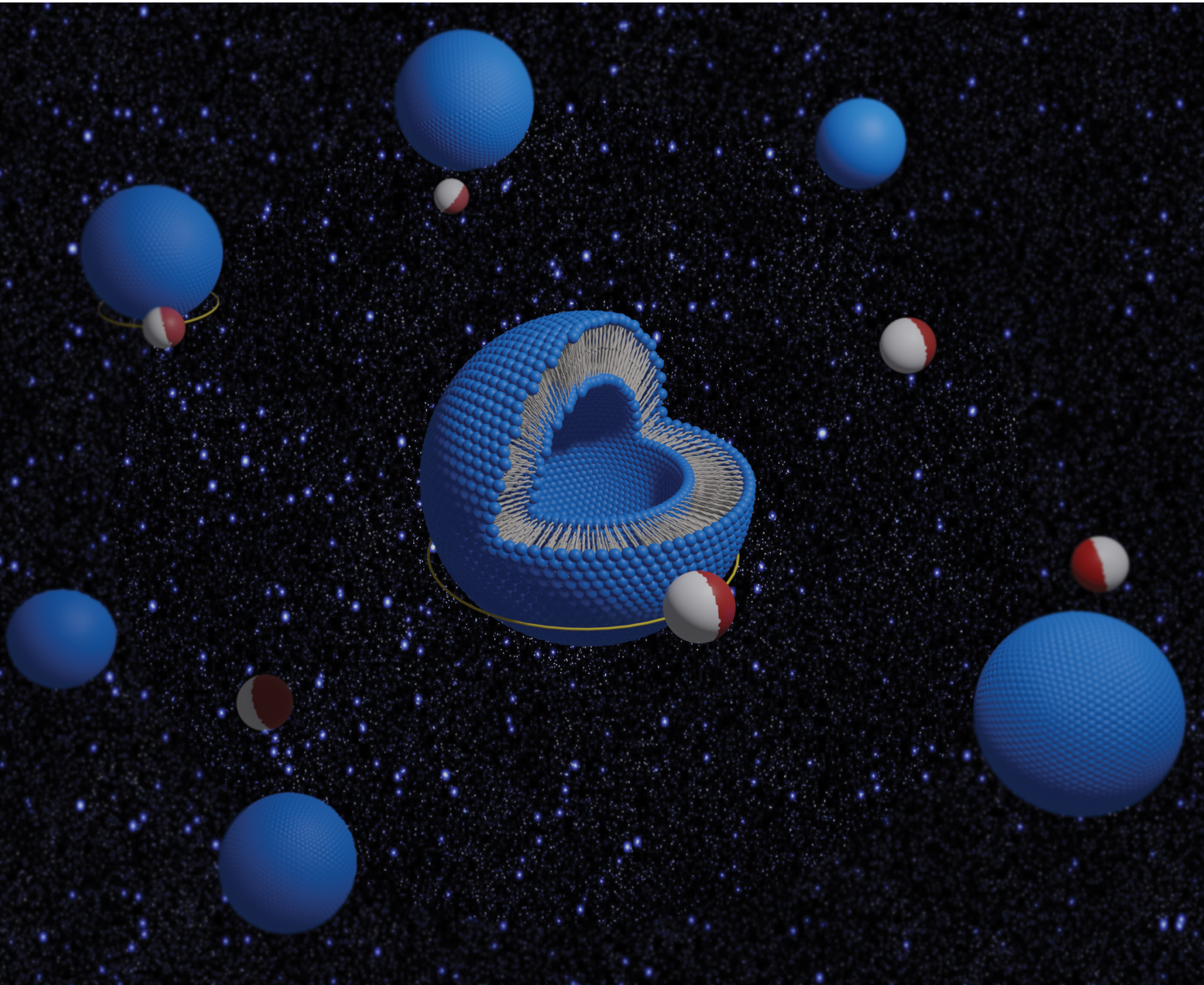


Soft Matter

rsc.li/soft-matter-journal



ISSN 1744-6848



Cite this: DOI: 10.1039/d0sm02183k

Active colloids orbiting giant vesicles†

Vaibhav Sharma, Elise Azar, Andre P. Schroder, Carlos M. Marques and Antonio Stocco *

Received 11th December 2020,
Accepted 1st March 2021

DOI: 10.1039/d0sm02183k

rsc.li/soft-matter-journal

Living or artificial self-propelled colloidal particles show original dynamics when they interact with other objects like passive particles, interfaces or membranes. These active colloids can transport small cargos or can be guided by passive objects, performing simple tasks that could be implemented in more complex systems. Here, we present an experimental investigation at the single particle level of the interaction between isolated active colloids and giant unilamellar lipid vesicles. We observed a persistent orbital motion of the active particle around the vesicle, which is independent of both the particle and the vesicle sizes. Force and torque transfers between the active particle and the vesicle is also described. These results differ in many aspects from recent theoretical and experimental reports on active particles interacting with solid spheres or liquid drops, and may be relevant for the study of swimming particles interacting with cells in biology or with microplastics in environmental science.

1. Introduction

Interaction of viruses, bacteria and other colloids with biological membranes plays a determinant role in many important processes such as microbial infections, drug delivery and toxicity from nanomaterials.¹ These processes are related to endocytosis, translocation and adsorption of living and artificial colloids in membranes. In biological cells, many passive and active (fuel-consuming) mechanisms² occur in the membrane during the recruitment of a particle inside the cell. Such mechanisms are often coupled together and are far from being understood today as shown by the COVID-19 pandemic.³ Beside membranes, motion of active and passive particles in many cases occurs close to solid walls, fluid interfaces and different kinds of obstacles.⁴ These obstacles not only act as a passive confinement but may also interact with the moving particle. As a function of the gap distance between the particle and the interacting interface, active particle motion can be strongly modified with respect to the motion inside an unbounded fluid. Hydrodynamic and long range surface forces together with specific interactions of the two interacting objects may promote new particle dynamics such as transport of cargo,⁵ orbital motion,⁶ reflection,⁷ constrained 2D^{8,9} and 1D directional motion.^{10,11}

Recently, Takagi *et al.* observed that active rod particles are captured by large solid colloidal spheres in orbital trajectories.⁶ They describe a number of observations pointing to a quite general

phenomena occurring for different active particle and obstacle sizes, even made of different materials. The trapping dynamics was modelled in terms of short-range hydrodynamic and steric interactions. In this experimental system, they also report no transfer of force or torque between the particle and the spherical obstacle during the orbital motion.⁶ Similar experimental observations were reported for active spherical Janus colloids moving in a crystal made of microparticles.¹² From a purely hydrodynamic viewpoint, these self-propelled Janus colloids can be described as “pusher” squirmers. Far-field hydrodynamic models have been developed to describe the dynamics of self-propelled particles moving close to a wall and interacting with solid or fluid obstacles in the bulk.^{13–15} In these models, only the fluid flow far (a fraction of the body length) from the self-propelled particle is described together with an hard core repulsion between the particle and the obstacle, which ensures that the particle cannot penetrate inside the obstacle.¹⁴ The flow far from the particle can be characterized without considering local effects due to the swimming mechanism details. In this case, the flow field is given by $\mathbf{u}(\mathbf{x}) = \alpha S_D(\mathbf{x} - \mathbf{x}_0; \hat{\mathbf{e}}) + O(|\mathbf{x} - \mathbf{x}_0|^3)$, where \mathbf{x}_0 and $\hat{\mathbf{e}}$ are the position and the orientation of the microswimmer respectively. S_D is the symmetric force dipole, and α is a coefficient. $\alpha > 0$ describes the flows generated by a “pusher” microswimmers: the flow is directed outward on the front and the back of the particle and inward on the side, which leads to an attraction between the swimmer and an obstacle located on the side. A threshold obstacle size, above which a persistent orbital motion occurs was always predicted by these models. Particle diffusion was also taken into account to describe the particle escape from the obstacle orbit.^{14,15}

Even in the absence of a spherical obstacle, the emergence of circular motion of self-propelled particles has been reported in various scenarios in the recent literature.^{16–23}

Institut Charles Sadron, CNRS UPR22—University of Strasbourg, 23 rue du Loess, Strasbourg, 67034, France. E-mail: stocco@unistra.fr

† Electronic supplementary information (ESI) available. See DOI: 10.1039/d0sm02183k

Here, we present experimental results on the dynamics of active Janus particles of spherical shape interacting with giant unilamellar vesicles (GUVs) made of phospholipid bilayers, which are an established biomimetic system for biological membranes. Both particles and GUVs are sedimented on the bottom substrate. To investigate the interaction between an active particle and a GUV, we have focussed our attention on the role of the particle activity in generating a self-propelled motion and on passive mechanisms such as the particle Brownian diffusion.

2. Material and methods

2.1. Active colloids

We used bare silica microspheres of radius $R_p = 1.98 \pm 0.05 \mu\text{m}$ and fluorescent Melamine Resin (MF) particles with $R_p = 1.15 \pm 0.06 \mu\text{m}$ (microParticle GmbH, Berlin, Germany). To fabricate Janus colloids, first we prepare a monolayer of silica/MF beads on a thoroughly cleaned silica wafer by drop casting (particle concentration is 0.2% by volume). After completely drying, a thin platinum layer is deposited by a metal sputtering technique (Edwards Auto 306 Evaporator).²⁴ The resulting particles are half coated with a thin platinum layer of $6 \pm 1 \text{ nm}$ thickness. This thickness was measured by light reflectivity (Multiskop, Optrel, Germany) on the corresponding planar surfaces.²⁵ Janus colloids are released from the wafer using 10 μL of glucose solution (0.1 M) along with gentle agitation using the pipet tip. As reported previously,⁹ the fabricated particles may present a variability in shape of the Janus boundaries and coating (see ESI,† Fig. S1).

2.2. Vesicle formation

Giant unilamellar vesicles, GUVs, are prepared using a PVA (Polyvinyl alcohol) gel assisted formation²⁶ which allows to fabricate vesicles with a high yield. PVA gel is prepared by dissolving PVA in PBS (Phosphate-Buffered Saline, 10 g L⁻¹) solution at 5% concentration. PVA gel is spread on a PTFE (Polytetrafluoroethylene) plate and dried for 30 minutes at 80 °C after. 10 μL of a 99 : 1 (molar) mixture of POPC (1-palmitoyl-2-oleoylphosphatidylcholine) and POPC-NBD (POPC fluorescently labelled with nitrobenzoxadiazole) lipids in chloroform (1 g L⁻¹) are spread on the PVA gel and vacuum dried for 15 minutes. The lipid system is then hydrated with 200 μL of sucrose (0.15 M) and allowed to grow for 2–3 hours. The vesicle suspension is then collected and sedimented in 1 mL of glucose (0.15 M) solution. The slight density mismatch between the sucrose solution inside the vesicle and the sucrose/glucose solution in the aqueous medium allows the vesicles to sediment at the bottom of the cell without strongly deforming the vesicle. A viscosity $\eta = 1.02 \text{ mPa s}$ of the sucrose/glucose solution was measured by passive microrheology.

2.3. Microscopy and tracking

Bright-field and fluorescence microscopy was used to observe Janus colloids and giant vesicles in aqueous media. 10 μL of a Janus particle dispersion and GUV solution along with 120 μL of glucose is filled in the sample cell. In all experiments with active colloids, a final concentration of 2% H₂O₂ (which is the

catalytic fuel of the Platinum Janus colloids), was used. Enough time (few minutes) is allowed to pass before observing the active motion of the colloids. At this hydrogen peroxide concentration no significant change of the GUV size distribution was observed (see ESI,† Fig. S2) and we did not observe any signature of hydrogen peroxide gradients in our experiments. The optical setup is a Nikon Eclipse TE2000 microscope ($\times 60$ objective) equipped with CMOS camera (Orca Flash 4.0, Hamamatsu). Videos were recorded in a 10–100 frame per second (fps) range. Particle tracking was done by the open source software Blender v 2.8. For the tracking of the vesicle centre of mass, ImageJ and Python routines were also used.

The obtained trajectories [t (s), x (μm), y (μm)] provide the particle/vesicle centre of mass position in time in the laboratory coordinate system.

3. Results and discussion

3.1. Orbital motion of Janus active colloids around isolated giant vesicles

For diluted enough particle and vesicle concentrations, we were able to observe the interaction between single active Janus colloids and single GUVs. The colloids are sedimented on the substrate, along which both passive and self-propelled motion occur. GUVs are also sedimented on the substrate without any strong adhesion between the solid wall and the membrane. A 2% H₂O₂ aqueous solution was always used to trigger the self-propulsion of the silica–platinum Janus colloids.^{27,28} In most of our experiments, whenever the trajectory of the active particle reached the vesicle boundary, the active particle initiated a striking orbital motion around the GUV. Fig. 1A shows a typical trajectory of an active colloid orbiting around a GUV observed (see ESI,† Video S1). For this particular example the GUV has a larger but comparable size to the active particle of radius $R_p \approx 2 \mu\text{m}$. For times $t < 1 \text{ s}$, the GUV is still not perturbed by the active particle. For $1 < t < 2 \text{ s}$, the silica face of the Janus particle pushes on the GUV membrane, which starts to translate a distance ΔL with approximately constant speed $V_{\text{GUV}} = 0.7 \mu\text{m s}^{-1}$. For $t > 2 \text{ s}$, the active particle performs a persistent orbital motion around the GUV.

Times spent by the particles in the GUV orbits vary from few seconds up to a thousand seconds. If enough time is allowed to pass, the active colloid eventually leaves the GUV orbit and initiates again an active “free” motion before encountering another GUV. Even if the Janus colloid seems to adhere to the GUV, with the Janus boundary oriented radially with respect to the GUV centre (Fig. 1A), no membrane deformation (partial membrane wrapping)¹ or adhesion was observed by fluorescence microscopy. Nanoscale membrane deformations below the resolution of our methods may however occur. By measuring the vertical positions of the GUV and particle equators (by detecting their respective focal planes using the z-stage of the microscope), we confirmed that both colloid and vesicle sediment at the bottom of the container, and the active motion of the Janus colloids occurs

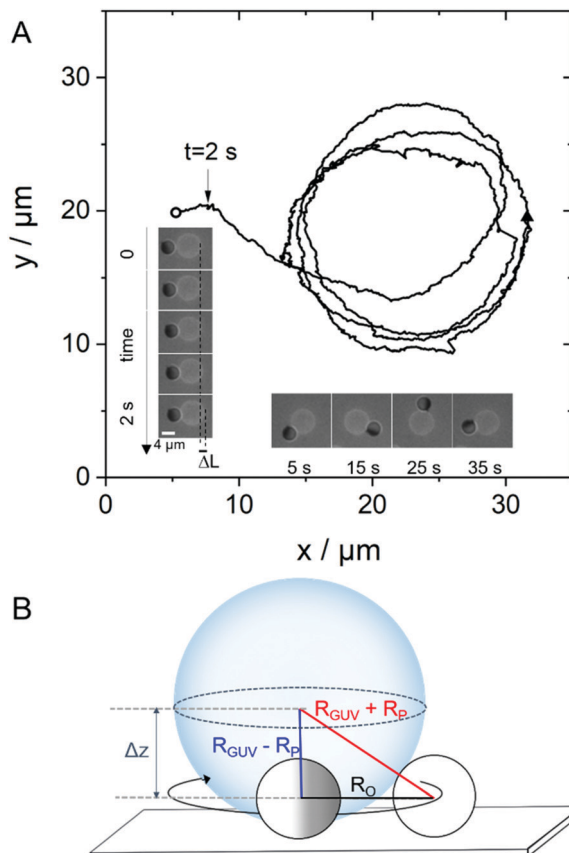


Fig. 1 (A) Centre of mass trajectory of an active colloid of radius $R_p \approx 2 \mu\text{m}$ interacting with a GUV. Time lapse images of the interaction between an active particle and a GUV are shown in the insets. (B) Sketch of the experimental geometry: a Janus colloid orbiting a GUV along the substrate. Δz is the difference between the focal plane of the GUV and the particle equator. R_o is the radius of the orbital trajectory (see also next figure).

in the wedge defined by the planar substrate and the GUV (see Fig. 1B).

Orbital trajectories were observed for both of the particle sizes that we used (MF, $R_p \approx 1 \mu\text{m}$ and silica, $R_p \approx 2 \mu\text{m}$) and in the whole range of GUV sizes investigated here. We observed both rotation directions with a comparable statistics between clockwise (CW) and counter clockwise (CCW) orbital motion directions.

For $R_p \approx 1 \mu\text{m}$ active colloids, in some cases, we also observed switching events between the two rotation directions during an ongoing orbital motion: an active colloid rotating CW (CCW) is able to remain close a GUV and change to CCW (CW) direction, without escaping the GUV, see Fig. 2 (two CCW-CW and one CW-CCW switching events). This switching may result from both in plane and out of plane Brownian rotational motion of the colloid.

For $R_p \approx 2 \mu\text{m}$ active colloids, instead, we did not detect switching events between the two possible orbital directions, see Fig. 2.

From the circular path of particle trajectories, one could evaluate an orbital radius R_o (see Fig. 1B and 2) and estimate the size of the GUV. Assuming spherical objects in close contact resting both on the planar substrate, $R_{\text{GUV}} \approx R_o^2/(4R_p)$. For some

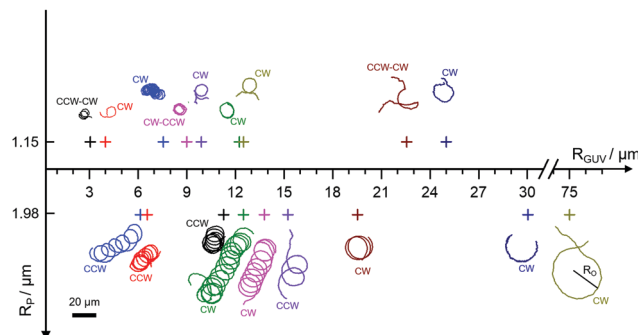


Fig. 2 Centre of mass trajectories of active Janus colloids ($R_p \approx 1$ and $2 \mu\text{m}$) around GUVs of different sizes. The time range of the observations is 30–788 seconds. Clockwise (CW) and counterclockwise (CCW) directions are also reported close to the trajectories.

trajectories we also measured directly the GUV size (in fluorescence or bright field microscopy) by changing the focal plane from the particle equator to the GUV. These GUV size measurements agree with the estimated value from the orbital radius. Preliminary Reflection Interference Contrast Microscopy (RICM) experiments show in some cases the signature of a vesicle flattening close to the substrate due to the gravity, which is however very small compared to the vesicle size.

Trajectories shown in Fig. 2 demonstrate that orbital motion occurs in a wide range of GUV and active particles sizes, covering vesicle to particle radii ratios $R_{\text{GUV}}/R_p \approx 1.5$ to 20. Note that some trajectories in Fig. 2 are clearly affected by some drift velocity due to convective flows. However, this drift velocity is significantly lower than the particle speed and it can be easily decoupled from the particle motion in our analysis.

We observe that active colloids display persistent orbital motion around GUVs, that can be viewed as soft spheres with fluctuating surfaces, a feature also seen for active rod particles orbiting around isolated solid obstacles; and for spherical active Janus colloids orbiting in a crystal made of large solid particles.^{6,12} In the bulk, far-field hydrodynamics is able to explain such persistent orbital motion for active particles behaving as a “pusher” squirmers. This squirmer category pushes the liquid in the front and in the rear, and entrain the liquid on the sides (here the Janus boundary), which leads to an effective hydrodynamic attraction with an obstacle (here the GUV) located in close proximity.^{6,14}

However, our experimental results for sedimented active colloids and GUVs show also a clear difference with respect to the bulk far-field hydrodynamic predictions for orbital motion around either spherical solid or liquid obstacles.^{6,14} In fact, in our experimental system we did not observe any critical radius of the GUVs for the onset of the orbital motion (see ESI,† Fig. S3). Hydrodynamic models predict that in the bulk, for obstacle size lower than a critical value R_c (≈ 10 – $15R_p$), the active particle shows a scattering behaviour; whilst for obstacle radii larger than R_c , a persistent orbital motion of the active particle around the obstacle occurs.

Analysing about two hundred trajectories showing the interaction between an active colloid and a GUV, we evaluate the

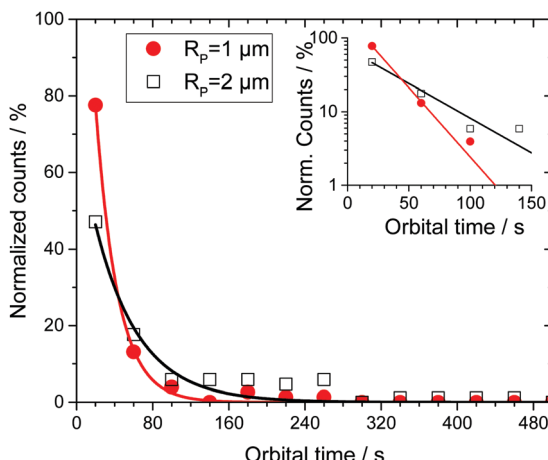


Fig. 3 Normalized counts of orbital times of $R_p \approx 1$ and $2 \mu\text{m}$ particles rotating around GUVs. The red and black curve are exponential functions $\sim \exp(-t_{\text{orb}}/t^*)$. A log-linear representation of the data is shown in the inset.

time spent by the particle around the GUV, which we call the orbital time (t_{orb}). In Fig. 3, we plot the normalized counts of orbital time t_{orb} (or trapping time¹⁴) for both particle sizes. It varies from few seconds to several minutes. An exponential function $\sim \exp(-t_{\text{orb}}/t^*)$ can be used to approximately describe the t_{orb} distribution.⁶ From the fits, we find characteristic times $t^* = 23 \pm 1 \text{ s}$ for $R_p \approx 1 \mu\text{m}$ and $t^* = 46 \pm 5 \text{ s}$ for $R_p \approx 2 \mu\text{m}$ (see inset in Fig. 3). It is important to remark that t^* for $R_p \approx 2 \mu\text{m}$ particles is approximately twice that of $R_p \approx 1 \mu\text{m}$ particles. Interestingly, this proportionality correlates thus with the bulk translational friction coefficient of spheres $6\pi\eta R_p$. It is thus tempting at this stage to speculate on the possible reasons for a particle to escape the orbit where it has been captured. The strength of the attraction of a pusher to a wall is known to depend on the velocity of the particle.¹⁰ A significant slowdown of the orbital velocity could then allow for escaping the orbit. However, all the escaping events that we have observed were not associated with a stalling or a significant reduction of the particle velocity. Another possible explanation for orbital escape could reside on the spontaneous stochastic rotation of the particle into an angular position where its propulsion would drive it away from the membrane.¹⁴ Indeed, as we will further study below, the orbital motion of the Janus pusher proceeds with a propulsion direction close to the tangent of the circular orbit, a strong deviation from this orientation could potentially drive the particle away. However, we have in a few instances observed clockwise movement spontaneously changing into counterclockwise, and conversely. During such changes of orbital direction, the particles are favorably oriented to move away from the wall but stay trapped instead. Hence, the escape dynamics may be governed by the Brownian translational diffusion of the particle as predicted by Spagnolie *et al.*,¹⁴ or by the membrane-particle repulsive interaction observed in the absence of H_2O_2 . Indeed, our passive colloids do not tend to adhere to GUVs in thermal Brownian motion, even when colloids were very close to the GUV membranes.

3.2. Active colloid–GUV interaction

In order to elucidate the strength and the nature of the interaction between an active colloid and a giant unilamellar vesicle, we performed a detailed analysis of the trajectories and of images taken during the orbital motion and compared them to data describing active colloids far away from the GUVs. From the active particle tracking, we calculated the discrete velocity vector $\bar{v} = (v_x, v_y)$ where $v_x(t) = \frac{x(t + \Delta t_1) - x(t)}{\Delta t_1}$, $v_y(t) = \frac{y(t + \Delta t_1) - y(t)}{\Delta t_1}$ and Δt_1 is the lowest time interval dictated by our camera detection, and its associated modulus $v = \sqrt{v_x^2 + v_y^2}$. From \bar{v} and v , discrete velocity vector $\langle \bar{v}(t + \Delta t) \cdot \bar{v}(t) \rangle = \langle v_x(t + \Delta t)v_x(t) \rangle + \langle v_y(t + \Delta t)v_y(t) \rangle$ and velocity modulus $\langle v(t + \Delta t)v(t) \rangle$ autocorrelation functions (VACF) were calculated. As reported for active colloids possessing both an active linear V and an angular ω velocities, the velocity autocorrelation function VACF of the instantaneous velocity \bar{v}_i in two dimensions can be written as:²⁹

$$\langle \bar{v}_i(t + \Delta t) \cdot \bar{v}_i(t) \rangle = 4D_{\text{tr}}\delta(\Delta t) + V^2 \cos(\omega\Delta t)f_r, \quad (1)$$

where the first term $4D_{\text{tr}}\delta(\Delta t)$ is related to the two-dimensional translational Brownian diffusion, D_{tr} ; and the second term $V^2 \cos(\omega\Delta t)f_r$, describes the active propulsion. If the active motion occurs in an unbound fluid (*i.e.* “free” motion), $f_r = \exp(-D_{\text{r}}\Delta t)$, and the bulk Brownian rotational diffusion, D_{r} , completely randomizes the persistent active motion at long time scales. Eqn (1) can be used for interpreting free trajectories even in the presence of experimental convection. Indeed, for $\Delta t > \Delta t_1$, VACF of the velocity \bar{v} can be written as the sum of the active propulsion term in eqn (1) and a constant drift velocity V_d (see Fig. 2):⁹

$$\langle \bar{v}(t + \Delta t) \cdot \bar{v}(t) \rangle = V^2 \cos(\omega\Delta t)f_r + V_d^2. \quad (2)$$

The orbital motion of the particle around a GUV is not in general described by eqn (1). The interactions of the particle with the vesicle introduces a number of other force sources. Beyond the particle propulsion (translation and rotation) and Brownian noise leading to the form in eqn (1): dynamical confinement forces and the resulting confined Brownian rotation and translation motions, vesicle shape fluctuations, all conjugate into a complex evolution of the particle orbital trajectory. It is however simple to show that for a perfectly circular orbital motion at constant orbital frequency ω , the autocorrelation function would have the form of eqn (1) with $f_r = 1$, thus providing a convenient manner to directly extract orbital velocities from the particle trajectory data alone.

In Fig. 4A, we show a typical trajectory of an active colloid orbiting around a GUV for about seven times (Orbit1). Then, the particle escapes from the first orbit and perform “free” active motion before encountering a second GUV (Orbit2). VACF corresponding to this trajectory divided in three ranges (Orbit1, Free and Orbit2) are shown in Fig. 4B.

In the orbital and “free” motion, $\langle v(t + \Delta t)v(t) \rangle$ as a function of the lag time is approximately constant, which shows the absence

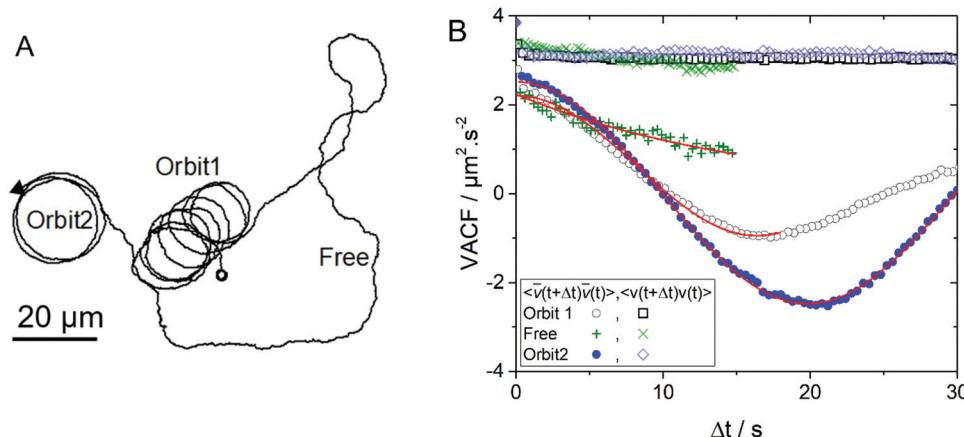


Fig. 4 (A) Trajectory of a $R_p \approx 2 \mu\text{m}$ active colloid orbiting around two GUVs and performing a “free” motion in between. (B) Velocity autocorrelation functions as a function of lag time Δt for the trajectory shown in (A).

of three-dimensional motion and negligible out of plane rotational dynamics of the active Janus colloid. A decay of the autocorrelation function of the active velocity modulus $v = \sqrt{v_x^2 + v_y^2}$ could in fact indicate a non-zero z -component of the velocity, v_z .⁸ $\langle \bar{v}(t + \Delta t) \cdot \bar{v}(t) \rangle$ in Orbit1 shows a clear oscillation due to the angular velocity ω . In Orbit1, damping of $\langle \bar{v}(t + \Delta t) \cdot \bar{v}(t) \rangle$ does not prevent the evaluation of the angular velocity. During the “free” motion, a decay of $\langle \bar{v}(t + \Delta t) \cdot \bar{v}(t) \rangle$ could be also fitted by eqn (2) with a zero angular velocity (no orbital motion), which also provides $f_r = \exp(-D_r \Delta t)$ and leads to the rotational diffusion in the “free” motion.

Fitting the data by eqn (2), we were able to evaluate, V and ω , and measure a negligible drift velocity ($<0.15 \mu\text{m s}^{-1}$). We evaluate ω in the range $0.25\text{--}0.76 \text{ rad s}^{-1}$ for $R_p \approx 1 \mu\text{m}$ and in between 0.15 and 0.5 rad s^{-1} for $R_p \approx 2 \mu\text{m}$ and verified that consistently $V = \omega R_O$ for all orbital motions. Moreover, rotational diffusions in the free motion $D_{r,\text{free}} = 0.10 \pm 0.03 \text{ rad}^2 \text{ s}^{-1}$ for $R_p \approx 1 \mu\text{m}$ and $D_{r,\text{free}} = 0.03 \pm 0.01 \text{ rad}^2 \text{ s}^{-1}$ for $R_p \approx 2 \mu\text{m}$ were obtained by the fits of eqn (2), which are comparable to the calculated bulk values $D_{r,\text{bulk}} = k_B T / (8\pi\eta R_p^3) = 0.11 \text{ rad}^2 \text{ s}^{-1}$ ($R_p \approx 1 \mu\text{m}$) and $D_{r,\text{bulk}} = 0.02 \text{ rad}^2 \text{ s}^{-1}$ ($R_p \approx 2 \mu\text{m}$).

In Fig. 5, we plot the particle speed in the orbit as a function of the speed when the active particle is far from the GUV (for each particle whose trajectory allows a robust measurement of $\langle v(t + \Delta t)v(t) \rangle = V^2$ in the “free” and orbital motion, see Fig. 4B). Even if the H_2O_2 fuel concentration is fixed at 2%, a range of velocities is observed due to different observation times (from few minutes to some hours after the addition of H_2O_2 , which is consumed in time) and an intrinsic variability in the catalytic coating due to the Janus colloid fabrication.⁹

Most of the data lies on the line $V_{\text{orb}} = V_{\text{free}}$, in agreement with results obtained for active rods orbiting around solid spherical obstacles, and pointing to a speed independent from the active particle-obstacle distance.⁶ However, for the velocities above $3 \mu\text{m s}^{-1}$, several points show $V_{\text{orb}} < V_{\text{free}}$. The equality of velocities in the free and orbital motions can be rationalized within two opposite scenarios. Obviously, velocity equality would hold if no additional dissipation was involved as the particle is

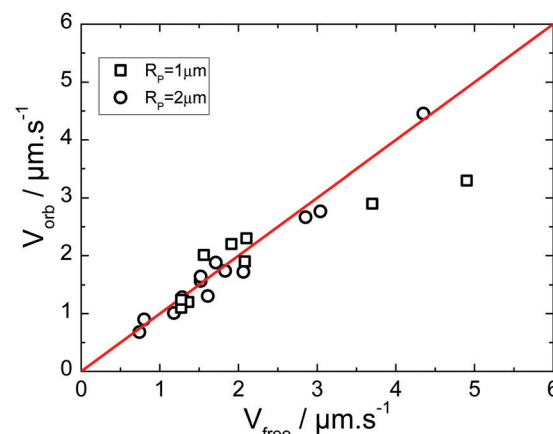


Fig. 5 Orbital speed of $R_p \approx 1 \mu\text{m}$ and $2 \mu\text{m}$ active colloids as a function of the speed far from the orbit.

captured into the orbital motion. However, this is unlikely due to the proximity to the membrane wall and to the strong distortion of the flow environment in the confinement wedge. $V_{\text{orb}} = V_{\text{free}}$ could also result from an increase of the propulsion mechanism due to a wall effect,¹⁰ which would be compensated by an increase of the translational drag.³⁰ Whether this perfect compensation is a coincidence or a consequence of the self-propelled motion confined wedges remains to be elucidated.

In order to gain a deeper insight into the rotational dynamics of an active colloid bound to an orbital trajectory, we performed image analysis of both the particle and the GUV around which it orbits. For some cases of $R_p \approx 2 \mu\text{m}$ particles, we were able to detect both the orientation of the particle Janus boundary and the centre of mass of the GUV (see ESI:[†] Videos S2 and S3). In this way, we could find the particle location angle θ and orientation angle φ in the GUV frame, see Fig. 6. Hence, to evaluate the Brownian rotational diffusion of the Janus particle in the orbit we calculated the mean squared angular displacement $\langle (\Delta\varphi - \theta)^2 \rangle$, which is plotted as a function of the lag time in Fig. 6B.

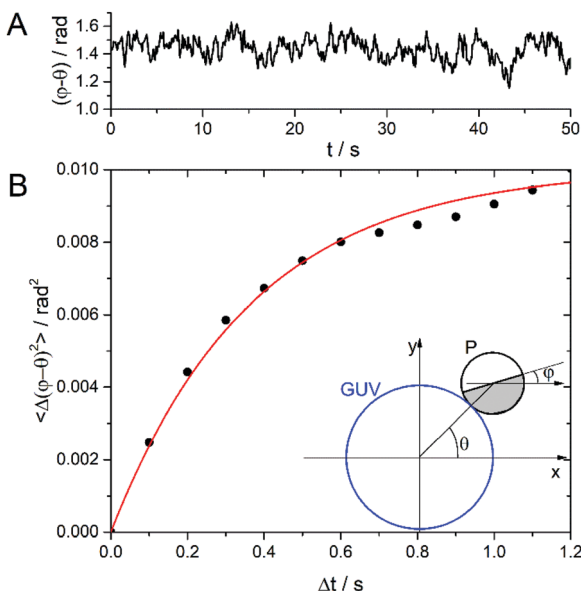


Fig. 6 (A) $\varphi - \theta$ as a function of the experimental time for a $R_p \approx 2 \mu\text{m}$ active colloid orbiting a GUV. (B) Mean squared angular displacement $\langle \Delta(\varphi - \theta)^2 \rangle$ as a function of the lag time. Solid line is a fit of eqn (3) to the data. In the inset, a sketch of a Janus particle (P) orbiting around a GUV together with the polar location angle θ and the orientation angle φ in the GUV frame are displayed.

For very short lag times, $\langle \Delta(\varphi - \theta)^2 \rangle$ shows a linear behaviour; whilst a saturation could be observed already before $\Delta t = 1 \text{ s}$, which is related to a confinement effect as also seen in Fig. 6A. Such saturation is the signature of confined rotational diffusion due to the fluid flow generated by the active particle, which tends to align the particle Janus boundary towards the GUV centre.¹⁴ For confined Brownian dynamics, $\langle \Delta(\varphi - \theta)^2 \rangle$ can be written as:¹⁰

$$\langle \Delta(\varphi - \theta)^2 \rangle = \frac{D_{r,\text{orb}}}{\Gamma} [1 - \exp(-2\Gamma\Delta t)], \quad (3)$$

where Γ is an effective elastic constant for the angular velocity: $\omega = -\Gamma(\varphi - \theta)$ which tends to restore the particle angular position $\varphi = \theta$ (see inset in Fig. 6B), with the particle Janus boundary orientated radially to the centre of the GUV.

The fit of eqn (3) to the data shown in Fig. 6B leads to $D_{r,\text{orb}} = 0.013 \pm 0.001 \text{ rad}^2 \text{ s}^{-1}$, which indicates a clear slowing down of the orbital rotational diffusion when compared to the theoretical $D_{r,\text{bulk}} = 0.02 \text{ rad}^2 \text{ s}^{-1}$ or the experimental $D_{r,\text{free}} = 0.03 \pm 0.01 \text{ rad}^2 \text{ s}^{-1}$. Moreover, for active particles interacting with a single wall, $\Gamma \cong V/R_p \cong 2.2 \text{ s}^{-1}$ was predicted by Das *et al.*, which is of comparable to $\Gamma = 1.15 \pm 0.09 \text{ s}^{-1}$ from the fit shown in Fig. 7. Hence, $\langle \Delta(\varphi - \theta)^2 \rangle$ data confirm a slowing down of the rotational diffusion with respect to the bulk rotational diffusion, which can be associated to a friction due to the active colloid–GUV interaction.

Force and torque transfers can indeed occur when an active particle interacts with a GUV. Already in Fig. 1, we showed that a GUV can translate a distance ΔL with a speed $V_{\text{GUV}} = 0.7 \mu\text{m s}^{-1}$ when an active colloid comes in close contact. An effective force F_{GUV} on the GUV can be calculated as $F_{\text{GUV}} = \zeta_{\text{tr}} V_{\text{GUV}} \approx 6\pi\eta R_{\text{GUV}} V_{\text{GUV}} \approx 46 \text{ fN}$, where ζ_{tr} is a simple estimate for the

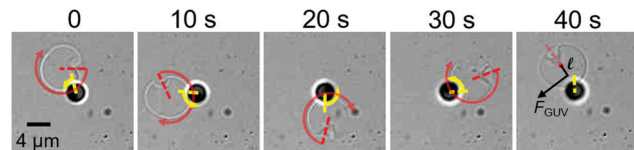


Fig. 7 Time lapse images of an $R_p \approx 2 \mu\text{m}$ active colloid rotating in a CCW direction (yellow arrow) but not translating and interacting with a GUV, which is both revolving around the Janus colloid and rotating in a CW direction (red arrow). Arrow arc length shows the rotation around its own axis between two frames (time is given on the top of the image).

GUV translational friction coefficient. These few tens of femtonewtons were measured several times in our experiments during the impact of active colloids on GUVs.

An additional experimental result is now presented to describe how an active colloid is able to impart also a torque on a GUV. Fig. 7 shows a complementary observation for an active colloid ($R_p \approx 2 \mu\text{m}$), which is not translating but only rotating in a CCW direction around an axis parallel to the normal to the substrate and passing through its centre of mass. Presumably, the colloid is partially stuck onto the solid substrate, but keeps its rotational activity. A GUV (whose size is approximately twice the particle size) revolves around the active Janus colloid also in a CCW direction. The GUV position appears to follow the orientation of the Janus boundary, with the centre of mass of the GUV slightly off with respect to the radial direction defined by the Janus boundary. Angular velocities of the GUV in the orbital motion and Janus colloid rotation are approximately the same, $\omega = 0.155 \pm 0.005 \text{ rad s}^{-1}$: a passive GUV is orbiting around an active colloid with a tangential velocity $V_{\text{GUV}} = \omega(R_{\text{GUV}} + R_p) \approx 0.9 \mu\text{m s}^{-1}$! An effective tangential force acting on the centre of mass of the GUV can be calculated as $F_{\text{GUV}} = \zeta_{\text{tr,GUV}} V_{\text{GUV}} \approx 72 \text{ fN}$. Some defects present on the GUV (see Fig. 7) also allow monitoring the rotation of the GUV around its own axis. The GUV rotates in a CW direction (opposite to the orbital motion) with $\omega_{\text{GUV}} = 0.415 \text{ rad s}^{-1}$, and a corresponding torque $M = \zeta_{\text{r,GUV}} \omega_{\text{GUV}} \approx 8\pi\eta R_{\text{GUV}}^3 = 41 \text{ fN } \mu\text{m}$, where ζ_r is the GUV rotational friction coefficient. The simultaneous force and torque acting on the GUV, generated by the local fluid flow of the active colloid, could be explained considering that the centre of mass of the GUV is slightly off with respect to the Janus boundary direction. An effective lever arm $\ell = M/F_{\text{GUV}} = 0.57 \mu\text{m}$ could thus describe the offset between the GUVs centre of mass and the location of the effective force acting on the GUV (see Fig. 7, 40 s).

To summarize, our experiments (Fig. 1, 6 and 7) clearly show the possible translation and rotation of GUVs under the effects of the fluid flows generated by the active particle. Note that our findings are in contrast to previous observations reporting no torque transfer and no rotation of solid spherical particle during the orbital motion of active rods.⁶

4. Conclusions

We have experimentally investigated at the single particle level, the interaction between an isolated active colloidal particle and

a giant unilamellar vesicle. Persistent orbital motion was observed in the whole range of GUV-particle size ratios investigated. Hence, no critical size for the onset of orbital motion was detected, which is in net contrast to far field hydrodynamic models for solid or fluid spherical obstacles in the bulk. In our experimental system, the tensionless and fluctuating nature of lipid bilayers leads to hydrodynamic boundary conditions that may be different to the ones considered so far.^{14,15} We also clearly show that a transfer of forces and torques occurs during the active colloid–GUV interaction, which results in a persistent translation of the GUV during the particle impact, a slowing down of the particle rotational diffusion with respect to the bulk, and a persistent GUV orbital motion around a rotating but not translating active particle. Still, far-field hydrodynamics can be used to explain not only the orbital motion due to a fluid flow generated by the active particle and pointing towards the particle Janus boundary, but also the role of the translational Brownian diffusion in the escape dynamics.^{14,15}

Finally, our results provide new perspectives on the interaction between active particles and soft compartments, which go beyond the effect of guiding¹¹ and scattering³¹ as observed for the interaction of a bacterium with a passive colloid. Active particles are indeed able to impart forces and torques on giant lipid vesicles, as it was very recently reported for active particles encapsulated inside a vesicle.³² These results motivate future investigations in partial and complete particle engulfment regimes to study directional transport of GUV by active colloids and activity triggered particle endocytosis.

Conflicts of interest

There are no conflicts to declare.

Acknowledgements

We thank Marc Schmutz for his help with the metal sputtering technique and the Electronic Microscopy platform of the Institut Charles Sadron. E. A. thanks the Emergence@INC of CNRS for financial support. V. S. acknowledges the Doctoral School ED 182 of University of Strasbourg for financial support.

References

- J. Agudo-Canalejo and R. Lipowsky, *ACS Nano*, 2015, **9**, 3704–3720.
- S. Zhang, H. Gao and G. Bao, *ACS Nano*, 2015, **9**, 8655–8671.
- W. C. K. Poon, A. T. Brown, S. O. L. Direito, D. J. M. Hodgson, L. Le Nagard, A. Lips, C. E. MacPhee, D. Marenduzzo, J. R. Royer, A. F. Silva, J. H. J. Thijssen and S. Titmuss, *Soft Matter*, 2020, 8310–8324.
- M. Safdar, J. Simmchen and J. Jänis, *Environ. Sci.: Nano*, 2017, **4**, 1602–1616.
- L. Baraban, M. Tasinkeyevich, M. N. Popescu, S. Sanchez, S. Dietrich and O. G. Schmidt, *Soft Matter*, 2012, **8**, 48.
- D. Takagi, J. Palacci, A. B. Braunschweig, M. J. Shelley and J. Zhang, *Soft Matter*, 2014, **10**, 1784–1789.
- W. E. Uspal, M. N. Popescu, S. Dietrich and M. Tasinkeyevich, *Soft Matter*, 2014, **1**, 1–15.
- X. Wang, M. In, C. Blanc, M. Nobili and A. Stocco, *Soft Matter*, 2015, **11**, 7376–7384.
- X. Wang, M. In, C. Blanc, A. Würger, M. Nobili and A. Stocco, *Langmuir*, 2017, **33**, 13766–13773.
- S. Das, A. Garg, A. I. Campbell, J. Howse, A. Sen, D. Velegol, R. Golestanian and S. J. Ebbens, *Nat. Commun.*, 2015, **6**, 1–10.
- J. Simmchen, J. Katuri, W. E. Uspal, M. N. Popescu, M. Tasinkeyevich and S. Sánchez, *Nat. Commun.*, 2016, **7**, 1–9.
- A. Brown, I. Vladescu, A. Dawson, J. Schwarz-linek, J. Lintuvuori and W. C. K. Poon, *Soft Matter*, 2016, **12**, 131.
- S. E. Spagnolie and E. Lauga, *J. Fluid Mech.*, 2012, **700**, 105–147.
- S. E. Spagnolie, G. R. Moreno-flores, D. Bartolo and E. Lauga, *Soft Matter*, 2015, **11**, 3396–3411.
- N. Desai, V. A. Shaik and A. M. Ardekani, *Soft Matter*, 2017, **14**, 264–278.
- H. Löwen, *Eur. Phys. J.: Spec. Top.*, 2016, **225**, 2319–2331.
- W. F. Hu, T. S. Lin, S. Rafai and C. Misbah, *Phys. Rev. Lett.*, 2019, **123**, 238004.
- N. Narinder, C. Bechinger and J. R. Gomez-Solano, *Phys. Rev. Lett.*, 2018, **121**, 078003.
- R. J. Archer, A. I. Campbell and S. Ebbens, *Soft Matter*, 2015, **11**, 6872–6880.
- F. Kümmel, B. ten Hagen, R. Wittkowski, I. Buttini, R. Eichhorn, G. Volpe, H. Löwen and C. Bechinger, *Phys. Rev. Lett.*, 2013, **110**, 198302.
- N. A. Marine, P. M. Wheat, J. Ault and J. D. Posner, *Phys. Rev. E: Stat., Nonlinear, Soft Matter Phys.*, 2013, **87**, 1–10.
- J. G. Gibbs and Y. P. Zhao, *Small*, 2009, **5**, 2304–2308.
- A. Girot, N. Danné, A. Würger, T. Bickel, F. Ren, J. C. Loudet and B. Pouliquen, *Langmuir*, 2016, **32**, 2687–2697.
- J. C. Love, B. D. Gates, D. B. Wolfe, K. E. Paul and G. M. Whitesides, *Nano Lett.*, 2002, **2**, 891–894.
- R. M. A. Azzam and N. M. Bashara, *Ellipsometry and Polarized Light*, North-Holland Publishing Company, 1987.
- A. Weinberger, F. C. Tsai, G. H. Koenderink, T. F. Schmidt, R. Itri, W. Meier, T. Schmatko, A. Schröder and C. Marques, *Biophys. J.*, 2013, **105**, 154–164.
- J. Howse, R. Jones, A. Ryan, T. Gough, R. Vafabakhsh and R. Golestanian, *Phys. Rev. Lett.*, 2007, **99**, 048102.
- J. G. Gibbs and Y.-P. Zhao, *Appl. Phys. Lett.*, 2009, **94**, 163104.
- S. Ebbens, R. A. L. Jones, A. J. Ryan, R. Golestanian and J. R. Howse, *Phys. Rev. E: Stat., Nonlinear, Soft Matter Phys.*, 2010, **82**, 015304.
- S. Villa, G. Boniello, A. Stocco and M. Nobili, *Adv. Colloid Interface Sci.*, 2020, **284**, 102262.
- A. Lagarde, N. Dagès, T. Nemoto, V. Démery, D. Bartolo and T. Gibaud, *Soft Matter*, 2020, **16**, 7503–7512.
- H. R. Vutukuri, M. Hoore, C. Abaurrea-Velasco, L. van Buren, A. Dutto, T. Auth, D. A. Fedosov, G. Gompper and J. Vermant, *Nature*, 2020, **586**, 52–56.

Supporting Information

Active Colloids Orbiting Giant Vesicles

Vaibhav Sharma, Elise Azar, Andre P. Schroder, Carlos M. Marques, Antonio Stocco^{*}

Institut Charles Sadron, CNRS UPR22—University of Strasbourg, 23 rue du Loess, Strasbourg,
67034, France

^{*}stocco@unistra.fr

Video S1. In a 2% H₂O₂ aqueous solution, a silica-platinum Janus colloid, $R_P \approx 2, \mu\text{m}$ self-propels towards a vesicle and is bound to an orbital trajectory around the GUV. The active particle approaches the vesicle and pushes it for the first seconds before advancing to an orbital motion. The black region corresponds to the platinum region of the particle.

Video S2. A silica-platinum Janus colloid, $R_P \approx 2 \mu\text{m}$, interacting with a giant lipid vesicle, $R_{\text{GUV}} \approx 9.4 \mu\text{m}$ in a 2% H₂O₂ aqueous solution (video speed up 3 times). The active particle persistently rotates around the GUV, and eventually escapes the GUV orbit. The black region corresponds to the platinum region of the particle.

Video S3. Three dimensional rendering of the data of Video S2 created using a free open-source software POV-Ray. It consists of the exact particle trajectory, particle orientation and GUV location (speed up 3 times).

Section S1. Shape variability in Janus boundary.....2

Section S2. Effect of Hydrogen Peroxide on GUV size distribution.....3

Section S3. Orbital motion around vesicle4

Section S1. Shape variability in Janus boundary

Janus colloids partially coated with platinum are fabricated using a metal sputtering technique (Edwards Auto 306 Evaporator). Within this fabrication protocol, the platinum coating and the Janus boundary could exhibit a “wavy” or “bumpy” contour, see Figure S1. The roughness has a characteristic length scale of 20-40 nm in the platinum layer.

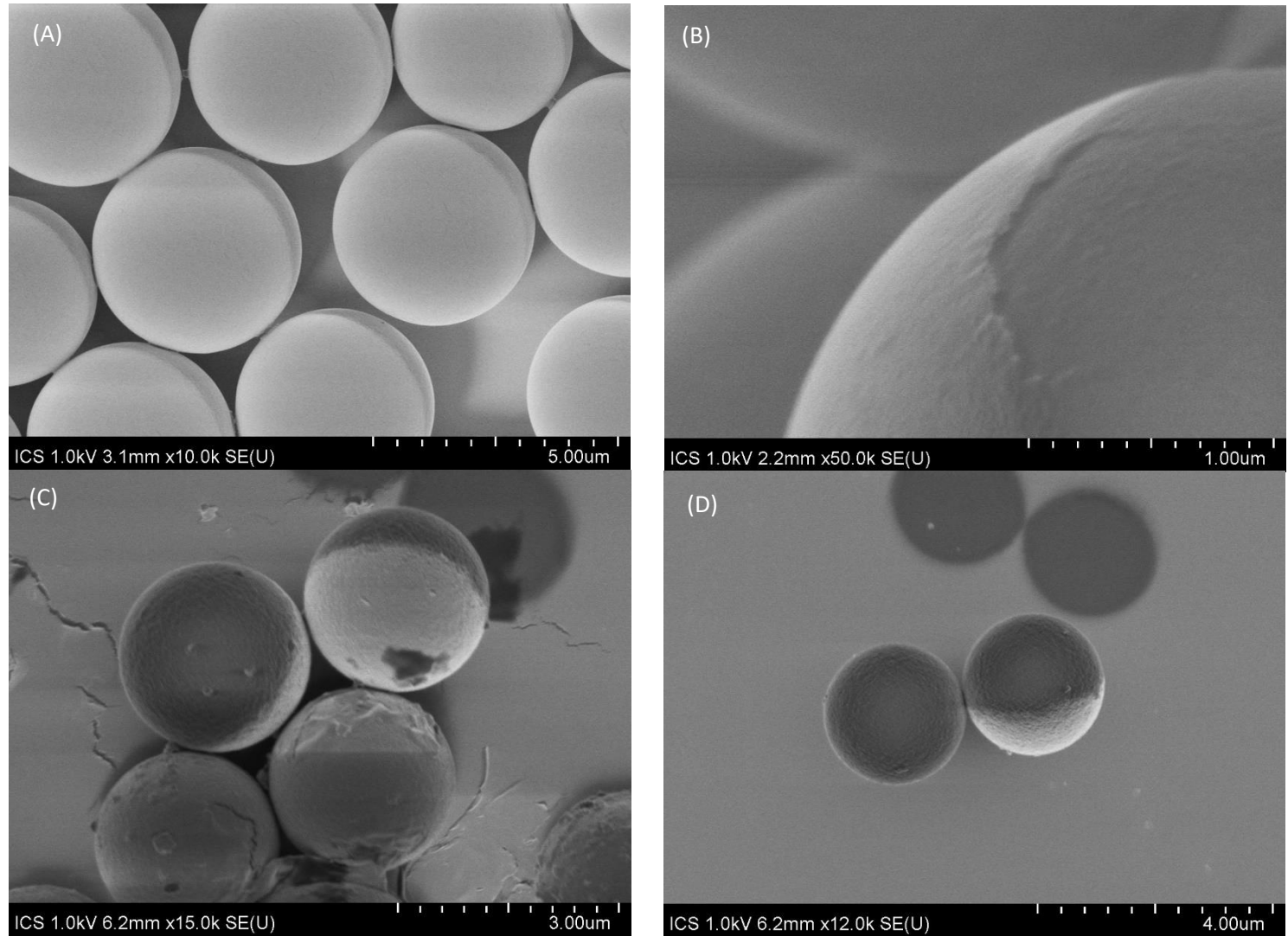


Figure S1. SEM images of $R_P \approx 2 \mu\text{m}$ (A and B) and of $R_P \approx 1 \mu\text{m}$. (C) and (D) Janus colloids showing the sizes and the shapes of the platinum coating.

Section S2. Effect of Hydrogen Peroxide on GUV size distribution.

The effect of 2% hydrogen peroxide (H_2O_2) on the size distribution of GUVs is shown in Figure S2. The sample was prepared with 10 μL of GUV solution along with 130 μL of glucose filled in a silicon isolator adhered to a clear glass slide. Multiple images panning around the entire sample in both bright-field and fluorescent conditions were recorded. The same protocol is repeated before and after adding H_2O_2 to the sample for multiple trials. 2% concentration of the H_2O_2 alone did not appear to cause any significant changes to neither the density nor the size distribution of the GUVs in the sample. As seen from Figure S2, the average size for the vesicle remains around $11 \pm 4 \mu\text{m}$ for long experimental times (up to 60 minutes).

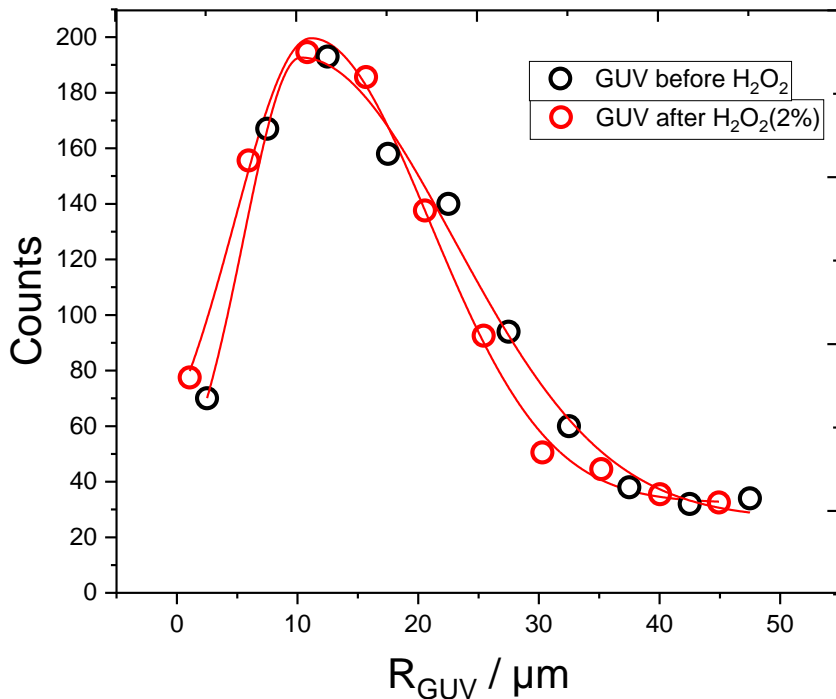


Figure S2. Size distributions of GUVs before and after the addition of hydrogen peroxide.

Figure S3 shows the orbital time as a function of the orbital radius (R_O) for all experiments where we could detect both the approach and escape time of an active particle interacting with an isolated vesicle. As already discussed in the main text, no critical orbital radius or vesicle radius was observed. Data shown in Figure S3 roughly follows the same statistics of the GUV size distribution shown in Figure S2.

Section S3. Orbital motion around vesicle

Figure S3 shows the orbital time as a function of the orbital radius (R_o) for all experiments where we could detect both the approach and escape time of an active particle interacting with an isolated vesicle. As already discussed in the main text, no critical orbital radius or vesicle radius was observed for the onset of the orbital motion. Data shown in Figure S3 roughly follows the same statistics of the GUV size distribution is shown in Figure S2.

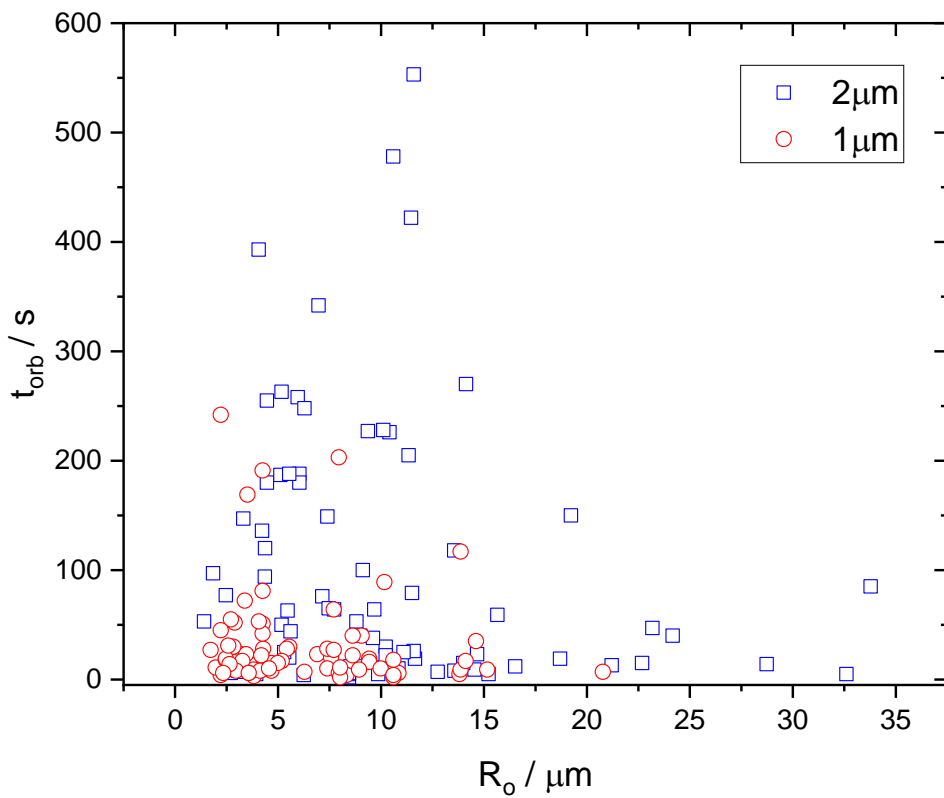


Figure S3. Orbital time versus orbital radius for $R_p \approx 1$ and 2 μm active colloids.